microscope. For the electron microscopy analysis, animals were fixed with glutaraldehyde and osmium tetraoxide (*34*). Five or six L4 or young adult animals were aligned within a small agar block, embedded, and sectioned together. Sections were poststained with uranyl acetate and lead citrate.
4. R. Durbin, thesis, University of Cambridge, Cambridge, England (1987).
5. G. Garriga, C. Desai, H. R. Horvitz, *Development* **117**, 1071 (1993).
6. S. Kim and W. G. Wadsworth, data not shown.
7. The *nid-1(RNAi)* animals were generated as described previously [A. Fire *et al.*, *Nature* **391**, 806 (1998)] by using a 1-kb sequence from exon 8, which was cloned into pBluescript (Stratagene) as template for RNA synthesis. RNA was produced by both T3 and T7 RNA polymerase, and the reactions were pooled before being injected into the intestines of *edIs20(unc-119::GFP)* transgenic animals. Phenotypes of the nervous system were observed under epifluorescence microscopy.
8. Seven PCR fragments, including the whole coding sequence and intron region, were amplified from the genomic DNA of *nid-1(ur41)* animals. PCR fragments were cloned into a pBluescript vector and subsequently sequenced by automatic sequencer. The mutation was confirmed by sequencing two independent PCR fragments.
9. U. Mayer, E. Kohfeldt, R. Timpl, *Ann. N.Y. Acad. Sci.* **857**, 130 (1998).
10. J. W. Fox *et al.*, *EMBO J.* **10**, 3137 (1991).
11. R. Timpl, J. C. Brown, *BioEssays* **18**, 123 (1996).
12. F. D. Yelian, N. A. Edgeworth, L. J. Dong, A. E. Chung, D. R. Armant, *J. Cell Biol.* **121**, 923 (1993).
13. R. F. Nicosia, E. Bonanno, M. Smith, P. Yurchenco, *Dev. Biol.* **164**, 197 (1994).
14. P. Ekblom *et al.*, *Development* **120**, 2003 (1994).
15. Y. Kadoya *et al.*, *Development* **124**, 683 (1997).
16. Immunostaining was performed by using freeze-fracture and methanol-acetone fixation as previously described (*35*). Polyclonal antibodies raised against mouse nidogen and a mouse monoclonal antibody against myosin heavy chain B (UNC-54) were used. For costaining, anti-rabbit fluorescein-conjugated and anti-mouse rhodamine-conjugated secondary antibodies were used.
17. Supplemental Web material is available at www.sciencemag.org/feature/data/1048303.shl
18. T. Sasaki, W. Gohring, T. C. Pan, M. L. Chu, R. Timpl, *J. Mol. Biol.* **254**, 892 (1995).
19. M. Hopf, W. Gohring, E. Kohfeldt, Y. Yamada, R. Timpl, *Eur. J. Biochem.* **259**, 917 (1999).
20. D. G. Moerman, H. Hutter, G. P. Mullen, R. Schnabel, *Dev. Biol.* **173**, 228 (1996).
21. P. L. Graham *et al.*, *J. Cell Biol.* **137**, 1171 (1997).
22. S. Kim, X. C. Ren, E. Fox, W. G. Wadsworth, *Development* **126**, 3881 (1999).
23. X. C. Ren, S. Kim, E. Fox, E. M. Hedgecock, W. G. Wadsworth, *J. Neurobiol.* **39**, 107 (1999).
24. Transgenic strains were generated by standard methods (*36*). pIM#194, an expression construct for *nid-1*, was constructed by cloning the 2.5-kb 5′ flanking region of *nid-1* into pPD 95.77 vector (from A. Fire). This GFP construct was coinjected at 10 μg/ml with pRF4 at 100 μg/ml. To establish a stable line, IM329 *urls151* [pIM#194, pRF4], transgenes were integrated by γ-ray irradiation. For the ectopic expression construct of *nid-1*, constructs pIM#195, pIM#196, and pIM#197, were made by using the 7-kb genomic *nid-1* coding region, which was amplified by high-fidelity PCR, ligated to Nhe I–Bgl II-digested vectors, pPD96.41, pPD49.83, and pPD96.52 (from A. Fire). These vectors contained 5′ flanking regulatory sequences of *mec-7*, *hsp16-41*, and *myo-3*, respectively (*36*). The *unc-119* regulatory sequence was amplified by using pIM175 as template (*23*), and cloned into the pPD49.26 vector (from A. Fire) to construct pIM#198. These constructs were injected at 10 μg/ml, with pRF4 into *nid-1(ur41); kyIs123 (zc21::GFP)* animals. The resulting strains are IM330 *urEx152* [pIM#195]; *nid-1(ur41); kyIs123(zc21::GFP)*; IM331 *urEx153* [pIM#196]; *nid-1(ur41); kyIs123 (zc21::GFP)*, IM332 *urEx154* [pIM#197]; *nid-1(ur41); kyIs123(zc21::GFP)*, IM333 *urEx155* [pIM#198]; *nid-1(ur41); kyIs123(zc21::GFP)*. Ectopic expression of *nid-1* was checked by in situ hybridization. IM331 embryos collected 1 to 6 hours after being laid were heat-shocked at 29.5°C for 1 hour. After heat shock, embryos were placed at 20°C, grown to the L4 stage, and examined for mispositioned nerves. Of those treated, 96% (n = 54) of the animals had wild-type nerves. For IM330, IM332, and IM333 animals, 32% (n = 41), 53% (n = 72), and 97% (n = 71) have wild-type nerves. Detection of RNA in whole-mount *C. elegans* embryos was performed as described (*37*). AP-anti-Dig antibody was used for alkaline phosphatase (AP)–mediated detection. 4′,6′-Diamidino-2-phenylindole (DAPI, 1 mg/ml) was included in the staining solution to allow nuclei to be identified by epifluorescence microscopy.
25. S. Kim and W. G. Wadsworth, data not shown.
26. A. Colavita, S. Krishna, H. Zheng, R. W. Padgett, J. G. Culotti, *Science* **281**, 706 (1998).
27. V. H. Hopker, D. Shewan, M. Tessier-Lavigne, M. Poo, C. Holt, *Nature* **401**, 69 (1999).
28. E. M. Hedgecock, J. G. Culotti, D. H. Hall, *Neuron* **4**, 61 (1990).
29. J. M. Kramer, R. P. French, E. C. Park, J. J. Johnson, *Mol. Cell. Biol.* **10**, 2081 (1990).
30. C. M. Coburn and C. I. Bargmann, *Neuron* **17**, 695 (1996).
31. A. C. Hart, S. Sims, J. M. Kaplan, *Nature* **378**, 82 (1995).
32. A. V. Maricq, E. Peckol, M. Driscoll, C. I. Bargmann, *Nature* **378**, 78 (1995).
33. E. R. Troemel, J. H. Chou, N. D. Dwyer, H. A. Colbert, C. I. Bargmann, *Cell* **83**, 207 (1995).
34. J. Sulston, E. Schierenberg, J. White, J. Thomson, *Dev. Biol.* **100**, 64 (1983).
35. W. G. Wadsworth, H. Bhatt, E. M. Hedgecock, *Neuron* **16**, 35 (1996).
36. C. Mello and A. Fire, *Methods Cell Biol.* **48**, 451 (1995).
37. G. Seydoux and A. Fire, *Methods Cell Biol.* **48**, 323 (1995).
38. We thank C. Bargmann, J. Culotti, E. Hedgecock, H. Hutter, and D. Pilgrim for generously providing GFP marker strains, P. Yurchenco for providing the nidogen antibodies, D. Miller for providing the UNC-54 antibody, the *Caenorhabditis* Genetics Center for strains, A. Coulson for cosmids, M. Driscoll, G. Patterson, J. Schwarzbauer, and P. Yurchenco for comments on the manuscript, Z. Altun-Gultekin, C.-C. Huang, G. Kao, Y.-S. Lim, P. Yurchenco, and Q. Wang for helpful discussions, R. Patel for assistance with electron microscopy, and X.-C. Ren for superb technical assistance.

20 December 1999; accepted 15 February 2000

Receptors for Dopamine and Somatostatin: Formation of Hetero-Oligomers with Enhanced Functional Activity

Magalie Rocheville,[1] Daniela C. Lange,[2] Ujendra Kumar,[1] Shutish C. Patel,[3] Ramesh C. Patel,[2] Yogesh C. Patel[1]*

Somatostatin and dopamine are two major neurotransmitter systems that share a number of structural and functional characteristics. Somatostatin receptors and dopamine receptors are colocalized in neuronal subgroups, and somatostatin is involved in modulating dopamine-mediated control of motor activity. However, the molecular basis for such interaction between the two systems is unclear. Here, we show that dopamine receptor D2R and somatostatin receptor SSTR5 interact physically through hetero-oligomerization to create a novel receptor with enhanced functional activity. Our results provide evidence that receptors from different G protein (heterotrimeric guanine nucleotide binding protein)–coupled receptor families interact through oligomerization. Such direct intramembrane association defines a new level of molecular crosstalk between related G protein–coupled receptor subfamilies.

In the brain, somatostatin (SST) is found in interneurons as well as projection neurons in different regions, and is thought to be an important physiological regulator of numerous functions (*1*). The actions of SST are mediated by a family of G protein–coupled receptors (GPCRs) with five subtypes, SSTR1 to SSTR5, that are widely distributed with high concentrations in the deeper cortical layers, the striatum, and most regions of the limbic system (*2*). Dopamine, like SST, acts through its own family of five GPCRs, D1R to D5R, that also display rich expression in the cerebral cortex, striatum, and limbic structures (*3*, *4*). The SSTR and DR families share ~30% sequence homology and appear to be structurally related. Behavioral and clinical evidence indicates an interaction between the somatostatinergic and dopaminergic systems (*5*–*8*). Intracerebroventricular injections of SST produce dose-dependent neurobehavioral changes progressing from hyperkinesia to catatonia (*6*). The dual excitatory and inhibitory effects occur through differential activation of postsynaptic or presynaptic DRs, respectively (*3*). Central administration of dopamine likewise activates both SST and SSTRs

[1]Fraser Laboratories, Departments of Medicine, Pharmacology, Therapeutics, Neurology, and Neurosurgery, McGill University and Royal Victoria Hospital, Montreal, Quebec H3A 1A1, Canada. [2]Departments of Physics and Chemistry, Clarkson University, Potsdam, NY 13699, USA. [3]VA Connecticut Healthcare System and New England Biomedical Research Center, Newington, CT 06111, USA.

*To whom correspondence should be addressed. E-mail: yogesh.patel@muhc.mcgill.ca

in the striatum (*7*).

We characterized the interaction between the long form of the human D2R and human SSTR5, a subtype previously reported to undergo ligand-dependent homodimerization and to form heterodimers with other SSTRs (human SSTR1) (*9*). DRs have also been shown to exist as dimers on the plasma membrane (*10*). Both receptors signal through inhibition of adenylyl cyclase via G_i proteins (*2, 3*). By immunocytochemistry, D2R and SSTR5 were colocalized in distinct neuronal subsets with the morphological characteristics of medium aspiny neurons in the striatum and pyramidal neurons in the cerebral cortex (Fig. 1) (*11*). We next investigated hetero-oligomerization of the two subtypes in a heterologous system by functional rescue of a partially active C-tail deletion mutant of human SSTR5 (Δ318 SSTR5) (*12*). This mutant displays complete loss of adenylyl cyclase coupling while retaining full agonist binding affinity. Δ318 SSTR5 was stably expressed in CHO-K1 cells either alone or with D2R. The mutant showed complete loss of the ability to inhibit forskolin-stimulated adenosine 3′,5′-monophosphate (cAMP) levels upon somatostatin-14 (SST-14) treatment (*12*). When coexpressed with D2R, however, SST induced dose-dependent inhibition of cAMP levels by the cotransfectants to a maximum 26 ± 2% at 10^{-6} M; this effect was completely abolished by pertussis toxin treatment (*12, 13*). Such functional complementation suggests that the Δ318 SSTR5 and D2R receptors associate as hetero-oligomers to constitute a functional G_i protein–linked effector complex. Treatment of the cotransfectants with dopamine produced 30 ± 2% reduction in cAMP. However, the addition of sulpiride (10^{-4} M), a dopamine receptor antagonist, completely abolished the ability of SST to inhibit forskolin-stimulated cAMP by Δ318 SSTR5-D2R putative hetero-oligomers. Such differential ability of agonist- or antagonist-bound D2R to rescue Δ318 SSTR5 could be explained by different conformational states of the agonist- or antagonist-occupied receptor and suggests a critical role of receptor conformation in promoting receptor association.

To investigate the interaction between wild-type receptors, we stably cotransfected D2R and HA-SSTR5 (human SSTR5 tagged at the NH_2-terminus with a nonapeptide of the hemagglutinin protein) in CHO-K1 cells to achieve levels of expression (maximum binding capacity B_{max} = 107 ± 29 fmol of protein per milligram for D2R, 163 ± 22 fmol/mg protein for HA-SSTR5) comparable to the density of endogenous receptor expression (*3, 13, 14*). Competition analysis of ^{125}I-labeled Leu^8-D-Trp^{22}-Tyr^{25}-SST-28 (LTT-SST-28) showed a 3000% increase in the binding affinity of SST-14 upon addition of the D2R agonist quinpirole (10^{-4} M) (from K_i 1.5 ± 0.2 nM to K_i 0.05 ± 0.01 nM, where K_i is the inhibition constant) (Fig. 2A). In contrast, addition of the DR antagonist sulpiride caused an 80% reduction in the affinity of SST-14 for binding to the putative HA-SSTR5–D2R oligomers (from K_i 1.5 ± 0.2 nM to K_i 7.5 ± 1.2 nM) (Fig. 2A). Because neither the dopamine agonist nor antagonist is capable of binding to HA-SSTR5 directly, these results suggest that the binding affinity of HA-SSTR5 for SST-14 is modulated by different conformational states of the agonist- or antagonist-occupied D2R through putative HA-SSTR5–D2R hetero-oligomers (Fig. 2A). Displacement analysis of ^{125}I-labeled spiperone binding by sulpiride showed a doubling of the affinity of sulpiride for the D2R in the presence of low SST concentrations (from K_i 17.2 ± 2.6 nM to K_i 8.2 ± 1.4 nM) (Fig. 2B). This suggests a synergistic role of SST on D2R affinity at low but not high concentrations because of a more suitable conformation for ^{125}I-labeled spiperone binding by putative HA-SSTR5–D2R hetero-oligomers.

G protein coupling of HA-SSTR5 and D2R was assessed by monitoring the effect of guanosine 5′-*O*-(3′-thiotriphosphate) (GTPγS) treatment on membrane ^{125}I-labeled LTT-SST-28 binding (Fig. 2C). GTPγS treatment of the cotransfectants led to a 41 ± 3% decrease in specific radioligand binding. Both dopamine

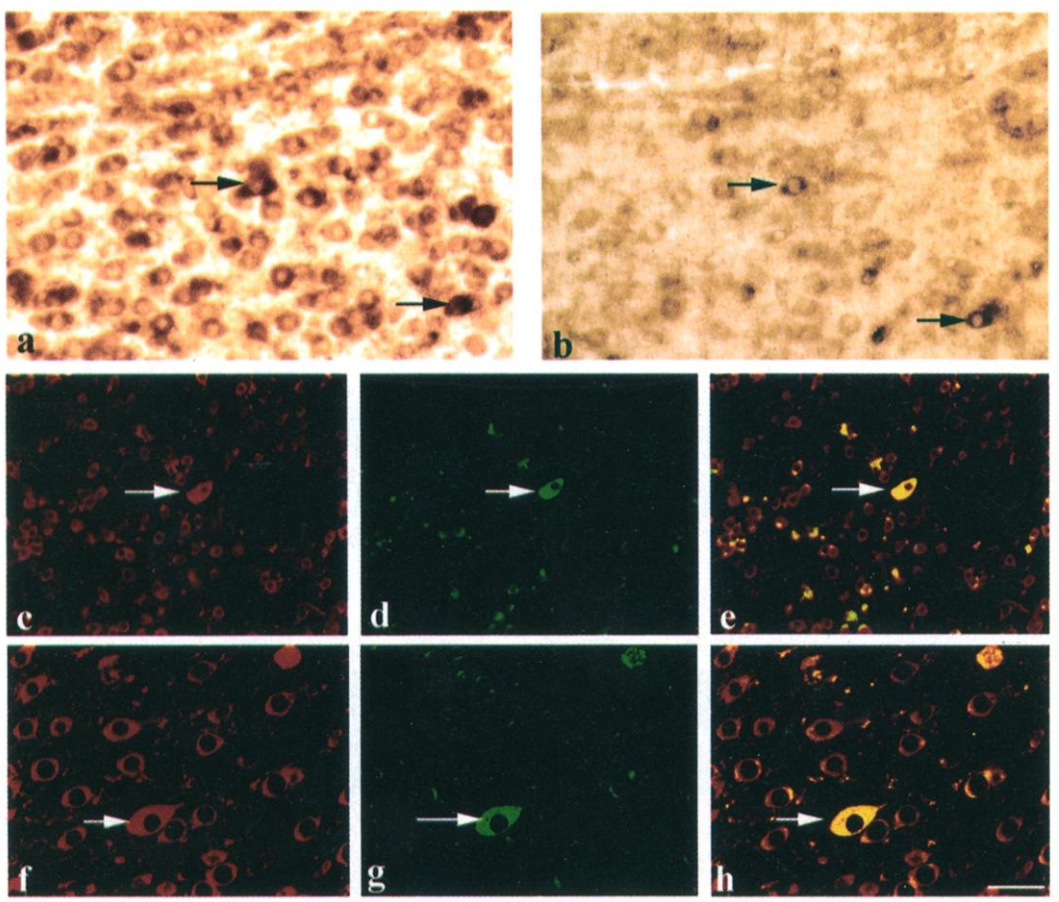

Fig. 1. Immunohistochemical colocalization of D2R and SSTR5 in rat brain cortex and striatum. (**A** and **B**) Serial sections of rat striatum showing many neurons expressing D2R (A). A subset of these neurons, with the morphological characteristics of medium aspiny neurons, show coexpression of SSTR5 (B). (**C** to **H**) Confocal images of striatal (C to E) and cortical (F to H) regions double-labeled for D2R and SSTR5. D2R is localized by Cy3 imaged in red fluorescence in (C) and (F). SSTR5-positive neurons are localized by FITC imaged in green and identified in the same section in (D) and (G). Coexpression of D2R with SSTR5 can be seen by the yellow-orange color in the merged images in (E) and (H). Scale bar, 25 μm.

and the dopamine agonist quinpirole increased inhibition by GTPγS. The dopamine antagonist eticlopride displayed no effect on SST-14–induced G protein coupling of HA-SSTR5, whereas sulpiride significantly reduced inhibition by GTPγS. Treatment of the cotransfectants with SST-14 or quinpirole induced maximum 36 ± 3% and 39 ± 3% inhibition of forskolin-stimulated cAMP, respectively (Fig. 2D). Simultaneous application of both agonists potentiated the cAMP inhibitory response to a maximum of 52 ± 4%. Sulpiride reduced SST-14–induced cAMP inhibitory response (maximum inhibition 25 ± 2%) and acted as a partial antagonist of SST-14 signaling.

To obtain direct evidence for association of SSTR5 and D2R in intact cells, we investigated receptor hetero-oligomerization by photobleaching fluorescence resonance energy transfer (pbFRET) microscopy (*15, 16*) (Fig. 3). In the basal state, we found a low effective FRET efficiency of 2 ± 2%, reflecting an insignificant amount of preformed hetero-oligomers (Fig. 4). Treatment with either SST-14 (10^{-6} M) or dopamine (10^{-4} M) resulted in a strong increase in FRET efficiency to 18 ± 2% and 16 ± 2%, respectively, suggesting that oligomerization of SSTR5 and D2R is induced by either agonist. Simultaneous treatment with both agonists (10^{-6} M SST-14 and 10^{-4} M dopamine) resulted in a similar FRET efficiency of 20 ± 2%. Treatment with the D2R-specific antagonists sulpiride (10^{-4} M) and eticlopride (10^{-4} M) led to a significantly lower FRET efficiency of 7 ± 2% and 3 ± 3%, respectively.

Our results demonstrate that D2R and SSTR5 associate on the plasma membrane and that receptors from different GPCR families can interact as functional oligomers. Although SSTR5 forms homodimers upon ligand activation as revealed by Western blots, and the D2R exists as preformed homodimers, it remains to be determined whether the two receptors assemble in vivo as simple heterodimers or larger oligomers. The D2R-SSTR5 oligomer is pharmacologically distinct from its receptor homodimers, as it is characterized by a much greater affinity for binding both dopamine and

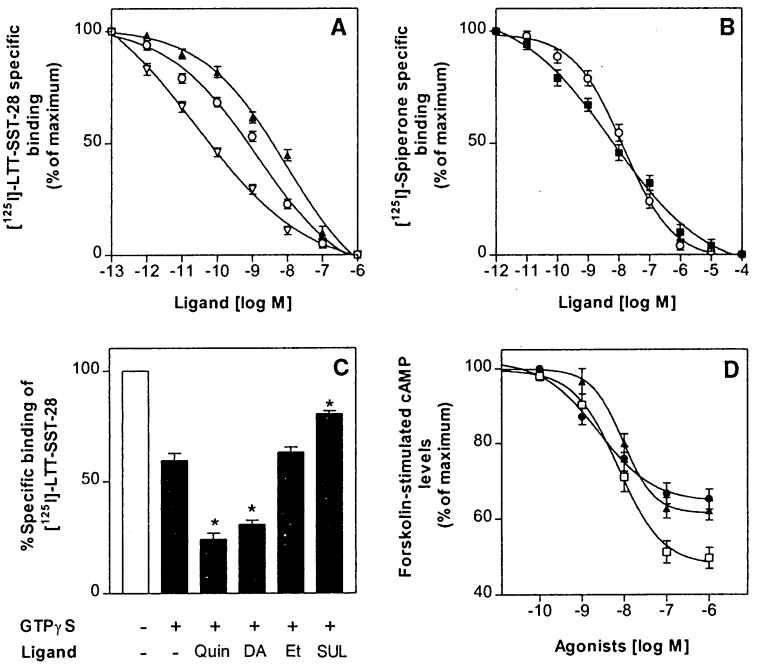

Fig. 2. Functional interaction of D2R with SSTR5. (**A**) Displacement analysis using the SSTR-specific ^{125}I-labeled LTT-SST-28 radioligand (*12, 13*). Membranes coexpressing HA-SSTR5 and D2R were treated with increasing amounts of SST-14 alone (open circles), SST-14 and quinpirole (10^{-4} M) (open triangles), or SST-14 and sulpiride (10^{-4} M) (solid triangles). DR ligand concentrations were selected to reach saturation binding, as well as maximal signaling (quinpirole) or inhibition of signaling (sulpiride). (**B**) Displacement analysis using the D2R-specific ^{125}I-labeled spiperone radioligand. Membranes coexpressing HA-SSTR5 and D2R were treated with increasing amounts of sulpiride alone (open circles) or sulpiride and SST-14 (10^{-6} M) (solid squares). The SSTR agonist concentration was selected to ensure maximal saturation binding and receptor signaling. (**C**) G protein coupling of the expressed receptors was assessed by investigating the effect on ^{125}I-labeled LTT-SST-28 binding of incubating membranes from cotransfectants with GTPγS (10^{-4} M) for 30 min at 37°C. Maximum specific binding obtained in the absence of GTPγS (open bar) was ~15%. SST-14 (10^{-6} M) was used to define nonspecific binding. GTPγS treatment significantly reduced specific binding of ^{125}I-labeled LTT-SST-28 to HA-SSTR5, reflecting G protein coupling. This response was enhanced by addition of quinpirole (Quin, 10^{-4} M) and dopamine (DA, 10^{-4} M), and was not affected by eticlopride (Et, 10^{-4} M) but was reduced by sulpiride (SUL, 10^{-4} M). Ligand concentrations used were chosen to reach saturation binding. (**D**) Receptor coupling to adenylyl cyclase (*12*) was assessed as inhibition of forskolin-stimulated cAMP after treatment of the cotransfectants with SST-14 (open circles), quinpirole (solid triangles), or SST-14 and quinpirole (open squares). Data are means ± SEM of three independent experiments. *$P < 0.01$ compared with control GTPγS treatment (Dunnett's post hoc one-way analysis of variance).

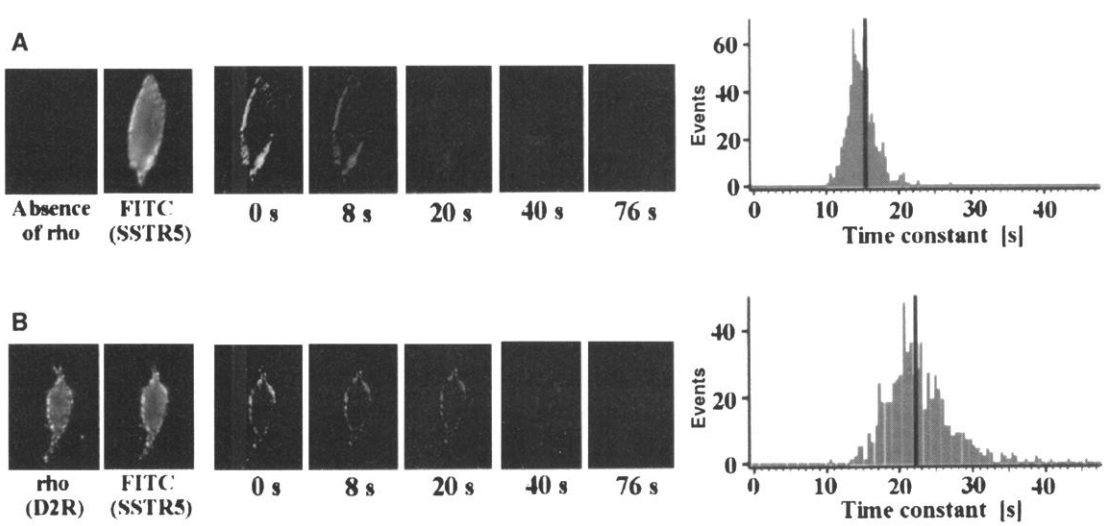

Fig. 3. Representative photobleaching experiment for treatment with SST-14 (10^{-6} M). (**A**) Photobleaching of donor in absence of acceptor (selection of images shown). Only the high-intensity membrane region was considered in analysis; low-intensity background and intracellular regions were masked (black). Two leftmost panels: Unmasked images showing absence of rhodamine and initial donor fluorescence. Right panel: Histogram of time constants obtained from single-exponential fits to pixel-based photobleaching decay curves. The average time constant of 15.8 s (solid bar) was taken as τ_{D-A}. (**B**) Photobleaching of donor in presence of acceptor. The presence of acceptor led to larger donor photobleaching time constants, with an average, τ_{D+A}, of 22.2 s, reflecting FRET between FITC and rhodamine.

SST agonists, and is associated with enhanced G protein and effector coupling to adenylyl cyclase. Hetero-oligomerization led to synergy such that the binding affinity for the second radioligand and signaling were increased as a result of receptor occupancy by the first ligand. Given the endogenous coexpression of D2R and SSTR5 in striatal and cortical neurons, hetero-oligomerization of the two receptors may be one explanation for the reported enhancement of dopaminergic and somatostatinergic transmission induced by in vivo administration of SST or dopamine agonists. While we have characterized the pharmacological properties of one DR-SSTR hetero-oligomer pair, there may be similar oligomeric interactions between other members of these two receptor families, which could explain the full range of functional biological interactions between the two transmitter systems.

There is increasing biochemical and functional evidence that a number of GPCRs exist as dimers or larger oligomers, and several models have been proposed to explain their regulation (*17*). The use of high-density recombinant receptor expression systems for detection of dimers by Western blots in several of these studies, however, could account for a high level of basal dimerization as an artifact of receptor overexpression. We have thus used lower density expression systems to mimic endogenous receptor expression levels, coupled with FRET analysis to monitor receptor oligomerization. The high sensitivity of FRET is ideally suited for studying molecular interaction at low expression level. pbFRET has been previously used to demonstrate oligomerization of the EGF receptor (*18*). Here we show that hetero-oligomerization of SSTR5 and D2R is also induced by ligand binding, that ligand binding to either receptor can trigger hetero-oligomer formation, and that there are no preformed hetero-oligomers in the absence of ligand. The results of FRET analysis complement the pharmacological data in showing that hetero-oligomerization induced by either SST or dopamine agonists goes hand in hand with activated receptor function. There was, however, no strict correlation between the level of oligomerization and the activity state of the receptor. Whereas pharmacological data demonstrated enhanced functional activity of the heteromeric receptor complex when occupied by both SST and dopamine ligands, no such synergy was found by FRET, which showed the same level of hetero-oligomerization for either agonist alone or both agonists applied together. Such dissociation is to be expected, given that FRET monitors only the presence of oligomers, not their activity state. Unlike SST and dopamine agonists, which both promoted D2R-SSTR5 hetero-oligomer formation, antagonists produced modest or no receptor oligomerization. Because no selective SSTR5 antagonists are currently available, we could not test the effect of antagonism at the SSTR5 receptor on D2R-SSTR5 hetero-oligomerization. Our results suggest a model in which agonist induces oligomerization, with the heteromeric receptor complex simultaneously occupied by two ligands being the most active signaling form. Antagonists may act by preventing hetero-oligomer formation or by promoting the formation of inactive hetero-oligomers. Hetero-oligomerization defines a new level of functional diversity in endogenous GPCR signaling. There are likely to be many such heteromeric GPCRs between members of different GPCR families that exist endogenously and that should constitute novel and hitherto unrecognized drug targets for combinations of agonists or antagonists, as well as for heterodimer-selective single-ligand molecules.

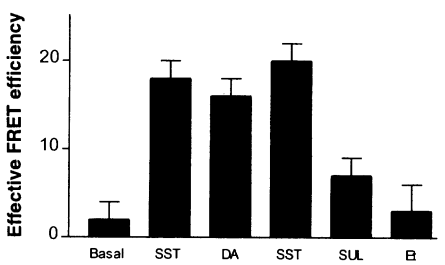

Fig. 4. Effective FRET efficiency in the basal state as well as after treatment with SST-14 (10^{-6} M), dopamine (10^{-4} M), SST-14 (10^{-6} M) plus dopamine (10^{-4} M), sulpiride (10^{-4} M), and eticlopride (10^{-4} M) on plasma membrane of CHO-K1 cells coexpressing HA-SSTR5 and wild-type D2R. Ligand concentrations were selected to reach saturation binding, as well as maximum signaling (agonists) or maximum inhibition of signaling (antagonists). The number of cells analyzed for each condition was ~45.

References and Notes

1. Y. C. Patel, in *The Role of Somatostatin*, vol. 4 of *Basic and Clinical Aspects of Neuroscience Series*, E. E. Muller, M. O. Thorner, C. Weil, Eds. (Springer-Verlag, Berlin, 1992), pp. 1–16; J. Epelbaum, *Prog. Neurobiol.* **27**, 63 (1986).
2. Y. C. Patel, *Frontiers Neuroendocrinol.* **20**, 157 (1999); D. Hoyer, H. Lubbart, C. Bruns, *Arch. Pharmacol.* **350**, 1 (1994).
3. C. Missale, S. Russel Nash, S. W. Robinson, M. Jaber, M. G. Caron, *Physiol. Rev.* **78**, 189 (1998); R. Picetti *et al.*, *Crit. Rev. Neurobiol.* **11**, 121 (1997).
4. D. M. Weiner *et al.*, *Proc. Natl. Acad. Sci. U.S.A.* **88**, 1859 (1991).
5. J. Chneiweiss, J. Glowinski, J. Premont, *J. Neurochem.* **44**, 1825 (1985).
6. M. T. Martin-Iverson, J. M. Radke, S. R. Vincent, *Pharmacol. Biochem. Behav.* **24**, 17 (1986); E. K. Havlick *et al.*, *Pharmacol. Biochem. Behav.* **4**, 455 (1976); R. Leblanc *et al.*, *Neurology* **38**, 1887 (1988); A. J. Kastin, D. H. Coy, Y. Jacquet, A. V. Schally, N. P. Plotnikoff, *Metabolism* **27**, 1247 (1978); M. L. Cohn and M. Cohn, *Brain Res.* **96**, 138 (1975).
7. R. M. Izquierdo-Claros, M. C. Boyano-Adanez, C. Larsson, L. Gustavsson, E. Arilla, *Brain Res. Mol. Brain Res.* **47**, 99 (1997); M. N. Rodriguez-Sanchez *et al.*, *J. Neurosci. Res.* **47**, 238 (1997).
8. P. Marzullo *et al.*, *Pituitary* **1**, 115 (1999).
9. M. Rocheville *et al.*, *J. Biol. Chem.* **275**, 7862 (2000).
10. G. Y. K. Ng *et al.*, *Biochem. Biophys. Res. Commun.* **227**, 200 (1996); S. R. George *et al.*, *J. Biol. Chem.* **273**, 30244 (1998).
11. Adult male CD rats were anesthetized with ketamine and perfusion-fixed, and 40-μm coronal sections of brain were processed for double-label immunocytochemistry. Antipeptide antibodies to the cytoplasmic tail of hSSTR5 or residues 231 to 244 of the third intracellular loop of human D2R were produced in rabbits, validated by Western blots, and used as primary antibodies [U. Kumar *et al.*, *Diabetes* **48**, 77 (1999)]. Sections were incubated with SSTR5 antibody (1:500) followed by incubation with fluorescein isothiocyanate (FITC)–conjugated antibody to rabbit immunoglobulin G (IgG) (1:100). The same sections were then exposed to D2R antibody (1:300), and receptor was visualized with Cy3-conjugated antibody to rabbit IgG (1:300). Because both primary antibodies were rabbit, the specificity of the immunofluorescent colocalization was validated by exposure of the SSTR5 labeled brain sections with the SSTR5 peptide immunogen for 3 to 4 hours at room temperature before incubation with D2R antibody. Coexpression of SSTR5 and D2R was also demonstrated independently in serial sections developed for SSTR5 and D2R localization by peroxidase immunocytochemistry.
12. N. Hukovic, R. Panetta, U. Kumar, M. Rocheville, Y. C. Patel, *J. Biol. Chem.* **273**, 21416 (1998).
13. Binding studies were carried out for 30 min at 37°C with 20 to 40 μg of membranes with subtype-specific radioligands (*12*). Receptor coupling to adenylyl cyclase was tested by incubating cells for 30 min with 1 μM forskolin with or without ligand at 37°C (*12*).
14. C. B. Srikant and Y. C. Patel, *Proc. Natl. Acad. Sci. U.S.A.* **78**, 3930 (1981).
15. Generally, FRET efficiencies are determined indirectly by measuring changes in the quantum yield of any competitive donor deactivation process upon introduction of an acceptor molecule (*16*). Donor photobleaching represents such a competitive process and was monitored during prolonged exposure to excitation light, both in the absence and in the presence of acceptor. The effective FRET efficiency E is calculated from the photobleaching time constants of the donor obtained in the absence (τ_{D-A}) and presence (τ_{D+A}) of acceptor according to

$$E = 1 - (\tau_{D-A}/\tau_{D+A})$$

The photobleaching decay was analyzed for the plasma membrane region on a pixel-by-pixel basis as well as averaged over the entire image. Image analysis procedures and instrumental setup are described in (*9*). CHO-K1 cells stably cotransfected with HA-SSTR5 and D2R were grown on glass cover slips for 24 hours, treated with agonists or antagonists for 30 min at 37°C, fixed, and processed for immunocytochemistry. HA-SSTR5 and D2R were specifically labeled with FITC and rhodamine, respectively, using mouse monoclonal HA antibodies and rabbit polyclonal antibodies followed by reaction with conjugated secondary antibodies. Both reactions resulted in specific plasma membrane staining.
16. T. Förster, *Naturwissenschaften* **6**, 166 (1948); T. M. Jovin and D. J. Arndt-Jovin, *Cell Structure and Function by Microspectrofluorometry* (Academic Press, New York, 1989); R. M. Clegg, in *Fluorescence Imaging Spectroscopy and Microscopy*, X. F. Wang and B. Herman, Eds. (Wiley-Interscience, New York, 1996).
17. B. A. Jordan and L. A. Devi, *Nature* **399**, 697 (1999); F. H. Marshall, K. A. Jones, K. Kaupmann, B. Bettler, *Trends Pharmacol. Sci.* **20**, 396 (1999); J. Wess and F. Y. Zeng, *J. Biol. Chem.* **274**, 19487 (1999); T. E. Hebert and M. Bouvier, *Biochem. Cell. Biol.* **76**, 1 (1998); S. Cvejic and L. A. Devi, *J. Biol. Chem.* **272**, 26959 (1997).
18. T. W. Gadella and T. M. Jovin, *J. Cell Biol.* **129**, 1543 (1995).

19. We thank H. H. Niznik for providing the cDNA for the long form of D2R, K. Koller for the cDNA for HA-SSTR5, and M. Correia for secretarial help. Supported by NIH grants NS32160-05 and NS34339 and Canadian Medical Research Council (MRC) grant MT-10411. Y.C.P. is a Distinguished Scientist of the MRC. M.R. is supported by a studentship from the Fonds de la Recherche en Santé du Quebec.

15 December 1999; accepted 22 February 2000